



A computationally efficient 3D Full-wave Model for coherent EM scattering from complex-geometry hydrometeors

Ines Fenni*, Ziad S. Haddad*, H el ene Roussel**, Kwo-Sen Kuo⁺, Raj Mittra#

* Jet Propulsion Laboratory, California Institute of Technology, USA ⁺ NASA GSFC/ESSIC, University of Maryland ** UPMC Univ Paris 06, France, # University of Central Florida, USA

1st International Summer Snowfall Workshop
28 – 30 June 2017

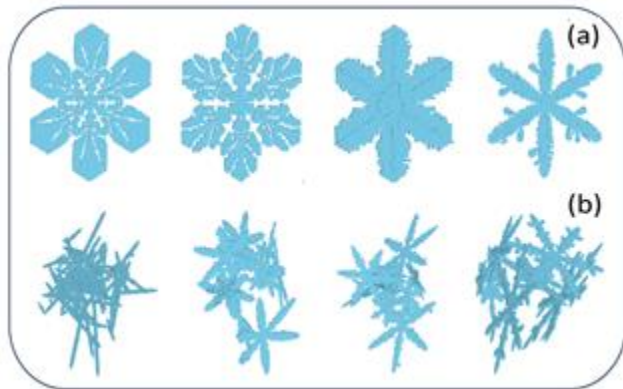
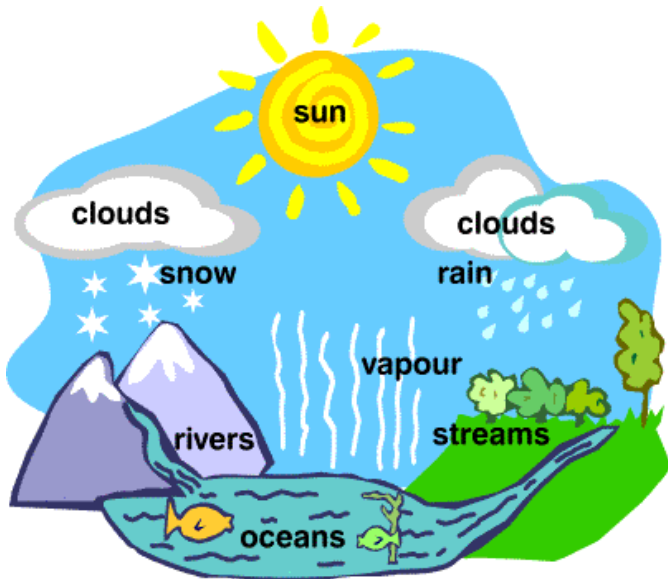


Application of CBFM to scattering by hydrometeors

Scattering by large and complex-shaped precipitation particles



Need to an **EM scattering model** to accurately calculate the scattering properties of inhomogeneous particles with complex geometries representing **snowflakes of various sizes and shapes**.

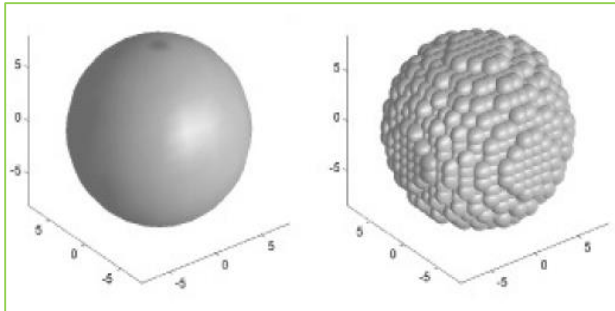


Pristine crystals (a) simulated using the Snowflake algorithm and aggregate snow particles (b) [1]

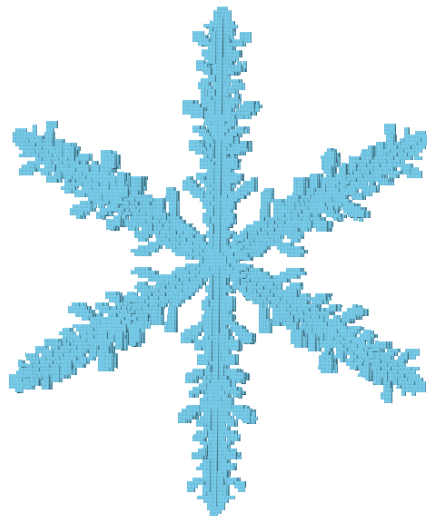
[1] Kuo, K. S., Olson, W. S., Johnson, B. T., Grecu, M., Tian, L., Clune, T. L., ... & Meneghini, R. (2016). The Microwave Radiative Properties of Falling Snow Derived from Nonspherical Ice Particle Models. Part I: An Extensive Database of Simulated Pristine Crystals and Aggregate Particles, and Their Scattering Properties. *Journal of Applied Meteorology and Climatology*, 55(3), 691-708.

Application of CBFM to scattering by hydrometeors

Scattering by large and complex-shaped precipitation particles



Discrete dipole approximation (DDA) representation of a sphere [2]



Star-shaped dendrite [1]



Need to an **EM scattering model** to accurately calculate the scattering properties of inhomogeneous particles with complex geometries representing **snowflakes of various sizes and shapes**.



A major drawback of the **Discrete Dipole Approximation** codes comes from the fact that if orientation averages are needed then computationally demanding linear equations must be solved repeatedly.

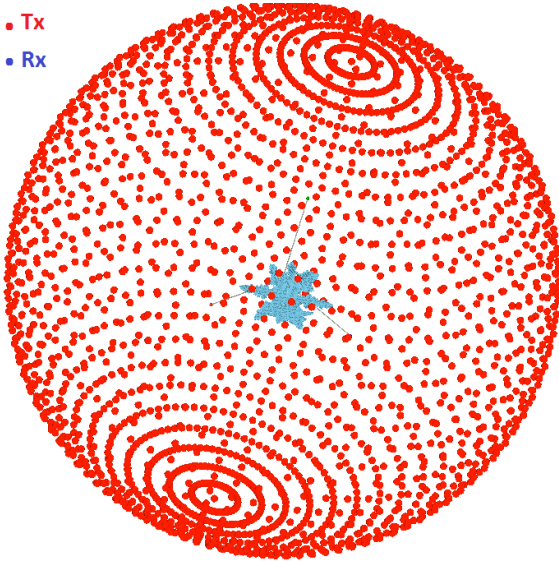
DDScat computes the orientational average $\langle Q \rangle$ of a quantity $Q(\beta, \theta, \phi)$ as

$$\langle Q \rangle = \frac{1}{8\pi^2} \int_0^{2\pi} d\beta \int_{-1}^1 d \cos \theta \int_0^{2\pi} d\phi Q(\beta, \theta, \phi)$$

[1] Kuo, K. S., Olson, W. S., Johnson, B. T., Grecu, M., Tian, L., Clune, T. L., ... & Meneghini, R. (2016). The Microwave Radiative Properties of Falling Snow Derived from Nonspherical Ice Particle Models. Part I ... Journal of Applied Meteorology and Climatology, 55(3), 691-708.

[2] B.T. Draine and P.J. Flatau, "Discrete-dipole approximation for scattering calculations," in JOSA A, 11(4), 1994, pp. 1491-1499.

- Tx
- Rx



Scattering by large and complex-shaped precipitation particles



Need to an **EM scattering model** to accurately calculate the scattering properties of inhomogeneous particles with complex geometries representing **snowflakes of various sizes and shapes**.



A major drawback of the **Discrete Dipole Approximation** codes comes from the fact that if orientation averages are needed then computationally demanding linear equations must be solved repeatedly.



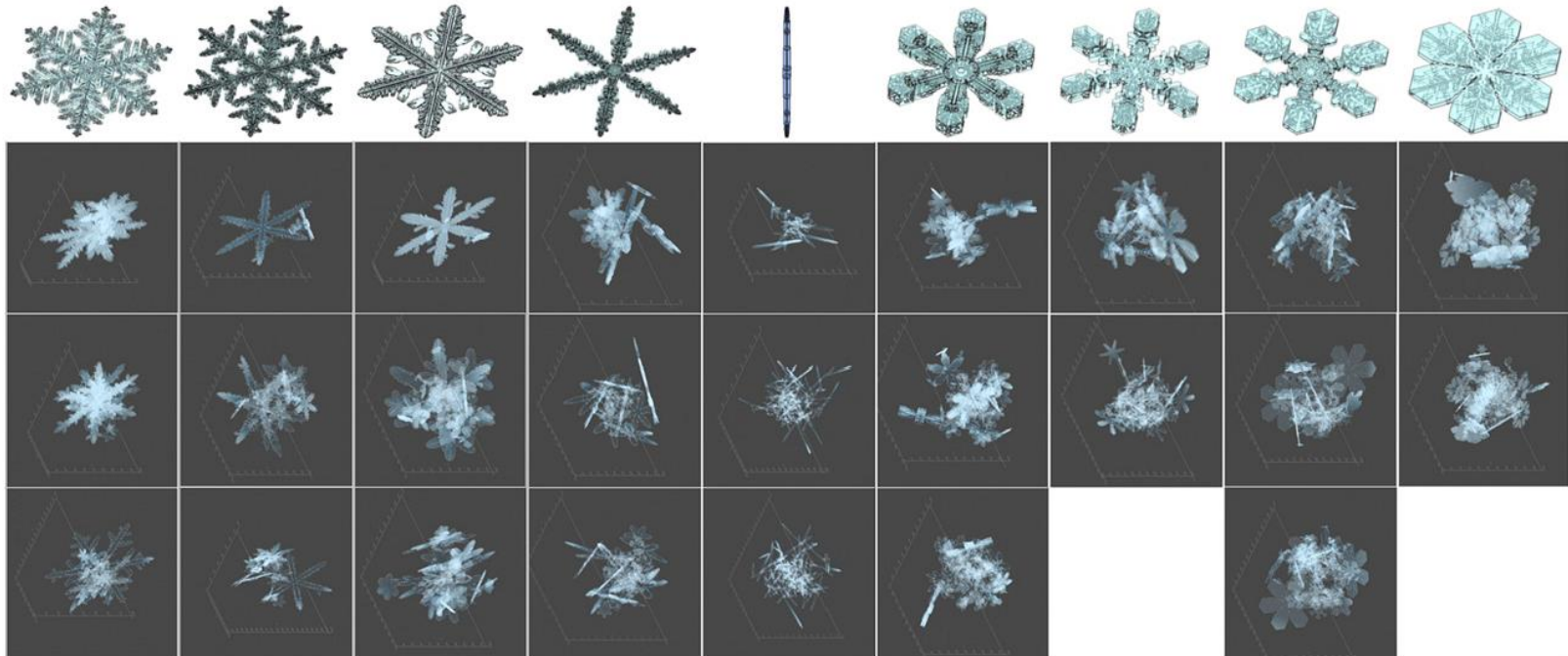
Characteristic Basis Function Method
(Direct Solver-based)

$$ZE = E^{inc}$$

Direct method

$$\langle Q \rangle = \frac{1}{4\pi} \int_0^{2\pi} d\phi_i \int_0^\pi \sin \theta_i d\theta_i Q(\phi_i, \theta_i)$$

OpenSSP database



(top) Pristine crystal types simulated using the snowflake algorithm [adapted from [Gravner and Griffeath \(2009\)](#)] Beneath each type are snapshots of the aggregation simulation that is based upon each crystal type.

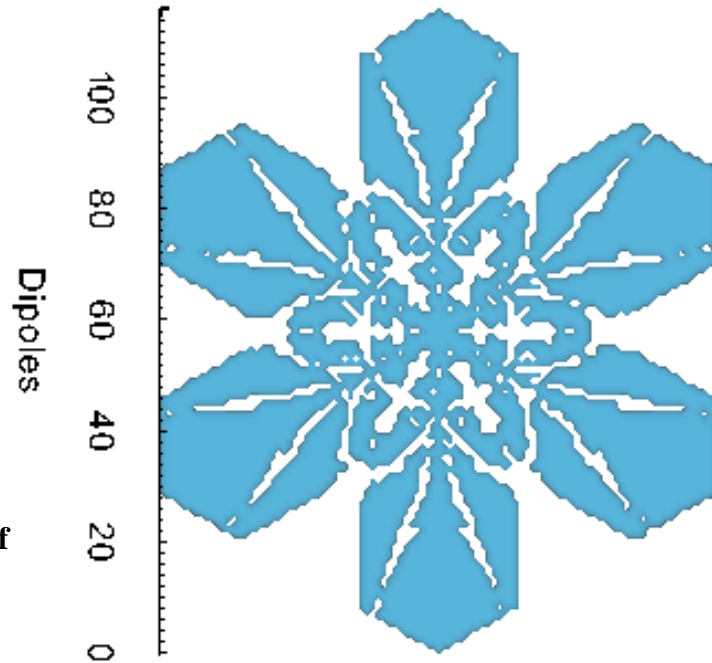
[1] Kuo, K. S., Olson, W. S., Johnson, B. T., Grecu, M., Tian, L., Clune, T. L., ... & Meneghini, R. (2016). The Microwave Radiative Properties of Falling Snow Derived from Nonspherical Ice Particle Models. Part I: An Extensive Database of Simulated Pristine Crystals and Aggregate Particles, and Their Scattering Properties. *Journal of Applied Meteorology and Climatology*, 55(3), 691-708.

- **6646 particles : single pristine crystals and aggregate snow particles**
- **50 μm resolution**

<ftp://gpmweb2.pps.eosdis.nasa.gov/pub/OpenSSP/>

VIEM/MoM-based 3D full-wave model

3D full-wave model, based on the volume integral equation method (**VIEM**)



Frequencies of interest :
(13 - 200 GHz)

Pristine crystal particle of
effective radius
 $a_p = 0.714476318$ mm

where $\chi(\vec{r}')$ is the dielectric contrast at the location r' , k_0 is the wavenumber in air and $\vec{G}(\vec{r}, \vec{r}')$ is the free space dyadic Green's function.

VIEM:
$$\vec{E}(\vec{r}) = \vec{E}^{inc}(\vec{r}) + (k_0^2 + \nabla\nabla \cdot) \int_{\Omega} \chi(\vec{r}') \vec{G}(\vec{r}, \vec{r}') \vec{E}(\vec{r}') d\vec{r}'$$



$$\vec{\Gamma} \vec{E}(\vec{r}) = \vec{E}^{ref}(\vec{r})$$

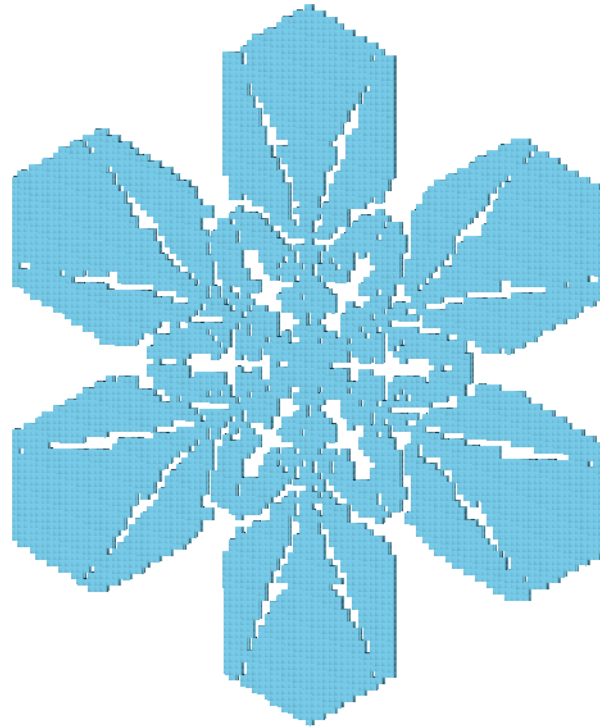
where
$$\vec{\Gamma} = \vec{I} - (k_0^2 + \nabla\nabla \cdot) \int_{\Omega} \chi(\vec{r}') \vec{G}(\vec{r}, \vec{r}') d\vec{r}'$$

VIEM/MoM-based 3D full-wave model

3D full-wave model, based on the volume integral equation method (VIEM)

Frequencies of interest :
(13 - 200 GHz)

Pristine crystal particle
of effective radius
 $a_p = 0.714476318$ mm
discretized into $Nb_c =$
12222 elementary cubic
cells



$$\bar{\Gamma} \bar{E}(\bar{r}) = \bar{E}^{ref}(\bar{r})$$

Method of Moments

The particle is discretized into N cubic cells Ω_n , of side c_n

$$c_n \geq \frac{\lambda_s}{10}; \lambda_s = \frac{\lambda_0}{\sqrt{Re(\epsilon_r)}}$$

$$\bar{E}(\bar{r}) = \sum_{n=1}^N \sum_{q=1}^3 E_q^n \bar{F}_q^n(\bar{r})$$

Use of dirac delta as test functions

To select a set of test functions W_p^m ($m=1, \dots, M$ and $p=x, y, z$), the point matching method is used. So, $M=N$ and W_p^m is a Dirac delta function located at the center of the cell Ω_n .

Use of piecewise constant basis functions

E_q^n is the constant unknown of \bar{F}_q^n , the n^{th} basis function for the component ($q=x, y$ or z) of the field inside the particle.

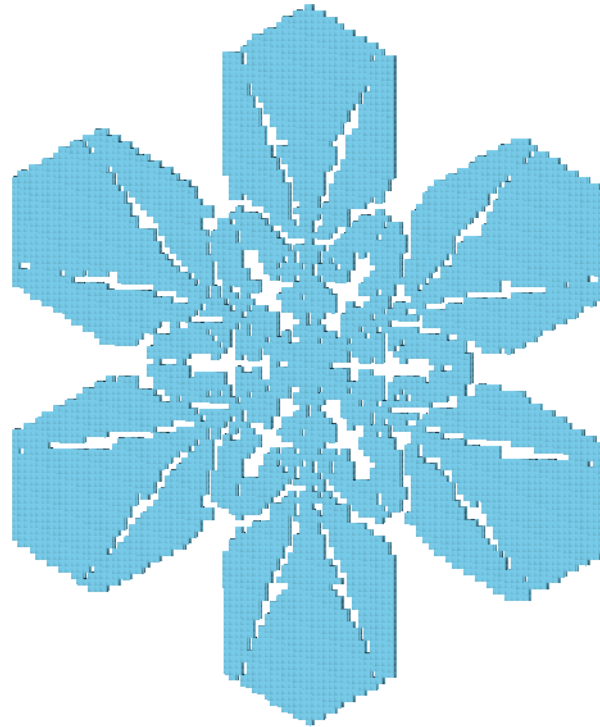
VIEM/MoM-based 3D full-wave model

3D full-wave model, based on the volume integral equation method (VIEM)

Frequencies of interest :
(13 - 200 GHz)

Pristine crystal particle
of effective radius
 $a_p = 0.714476318$ mm
discretized into $Nb_c =$
12222 elementary cubic
cells

Z is the $3Nb_c \times 3Nb_c$ full
matrix representing the
interactions between the
different cells.



$$\bar{\bar{E}}(\bar{r}) = \bar{E}^{ref}(\bar{r})$$

Method of Moments

The particle is discretized into N
cubic cells Ω_n , of side c_n

$$c_n \geq \frac{\lambda_s}{10}; \lambda_s = \frac{\lambda_0}{\sqrt{Re(\epsilon_r)}}$$

$$\bar{E}(\bar{r}) = \sum_{n=1}^N \sum_{q=1}^3 E_q^n \bar{F}_q^n(\bar{r})$$

$$Z E = E^{inc}$$

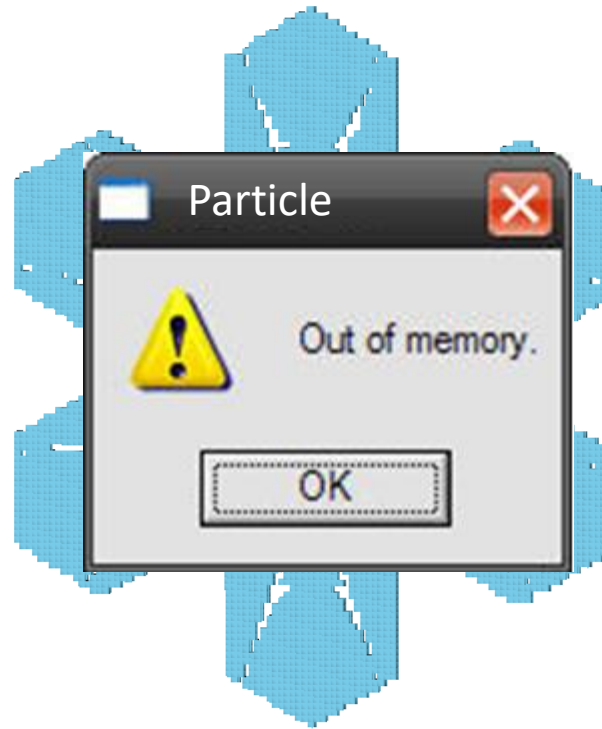
VIEM/MoM-based 3D full-wave model

3D full-wave model, based on the volume integral equation method (VIEM)

Frequencies of interest :
(13 - 200 GHz)

Pristine crystal particle
of effective radius
 $a_p = 0.714476318$ mm
discretized into $Nb_c =$
12222 elementary cubic
cells

Z is the $3Nb_c \times 3Nb_c$ full
matrix representing the
interactions between the
different cells.



$$\bar{\bar{E}}(\bar{r}) = \bar{E}^{ref}(\bar{r})$$

Method of Moments

The particle is discretized into N
cubic cells Ω_n , of side c_n

$$c_n \geq \frac{\lambda_s}{10}; \lambda_s = \frac{\lambda_0}{\sqrt{Re(\epsilon_r)}}$$

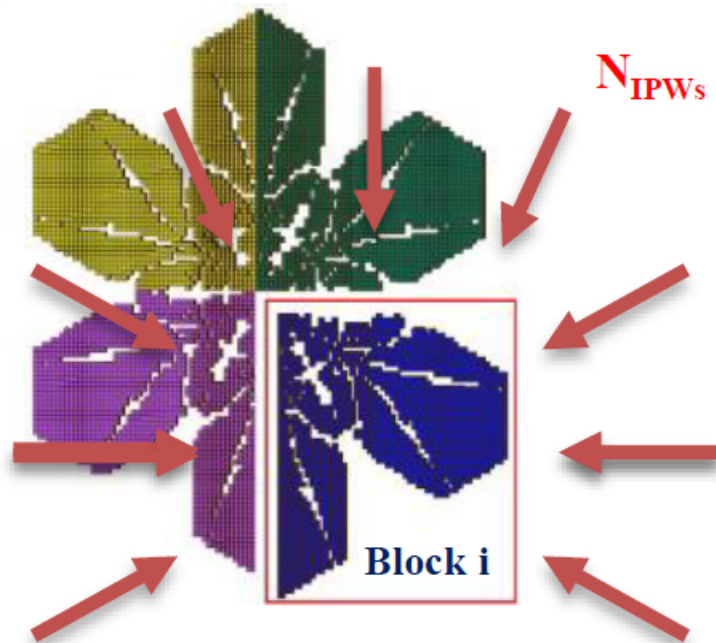
$$\bar{E}(\bar{r}) = \sum_{n=1}^N \sum_{q=1}^3 E_q^n \bar{F}_q^n(\bar{r})$$

$$Z E = E^{inc}$$

After dividing the 3D complex geometry of the precipitation particle of N cells into M blocks

1

Generation of the CBFs



$$Z^{ii} E_{MBFs}^{ii} = E_{IPWs}^{ii}$$

2

Computation of Z^c

Example : M = 4

$$Z^c = \begin{pmatrix} C^{(1)t} Z_{11} C^{(1)} & \dots & C^{(1)t} Z_{14} C^{(4)} \\ C^{(2)t} Z_{21} C^{(1)} & \dots & C^{(2)t} Z_{24} C^{(4)} \\ \vdots & \ddots & \vdots \\ C^{(4)t} Z_{41} C^{(1)} & \dots & C^{(4)t} Z_{44} C^{(4)} \end{pmatrix}$$

$$K = S_1 + S_2 + S_3 + S_4 \ll 3 * N$$

3

$$Z^c \alpha = E^{c,inc}$$

Application of the domain decomposition-based CBFM

After dividing the 3D complex geometry of the precipitation particle of N cells into M blocks

1 **Generation of the CBFs**

N_{IPWs}

Block i

$$Z^{ii} E_{MBFs}^{ii} = E_{IPWs}^{ii}$$

2 **Computation of Z^c**

Example : M = 4

$$Z^c = \begin{pmatrix} C^{(1)t} Z_{11} C^{(1)} & \dots & C^{(1)t} Z_{14} C^{(4)} \\ C^{(2)t} Z_{21} C^{(1)} & \dots & C^{(2)t} Z_{24} C^{(4)} \\ \vdots & \ddots & \vdots \\ C^{(4)t} Z_{41} C^{(1)} & \dots & C^{(4)t} Z_{44} C^{(4)} \end{pmatrix}$$

$K = S_1 + S_2 + S_3 + S_4 \ll 3 * N$

Compression Rate

$$CR = \frac{\text{size of } Z}{\text{size of } Z^c}$$



Application of the domain decomposition-based CBFM

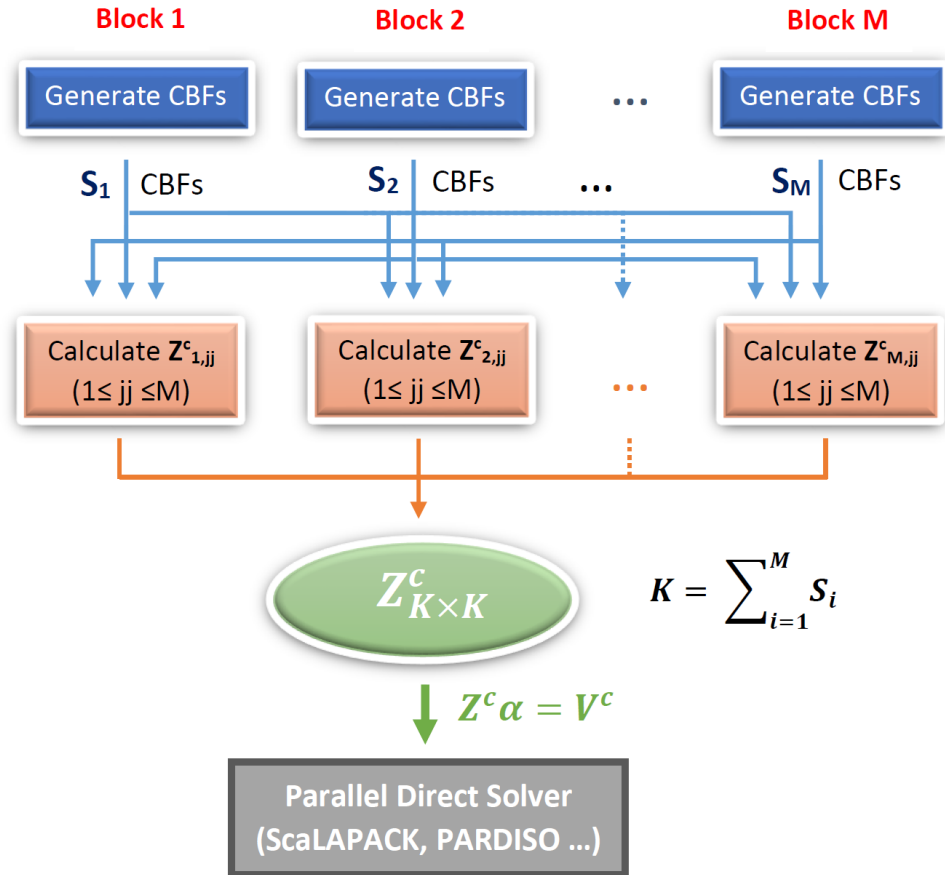
Comparison MoM/CBFM in terms of computing complexity

MoM : $O(3N)^3$

CBFM CBFs : $O(3N/M)^3$

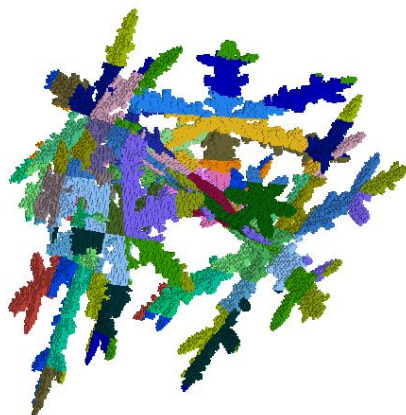
Z^c : $O(3N \times K)$

$(Z^c)^{-1}$: $O(K)^3$

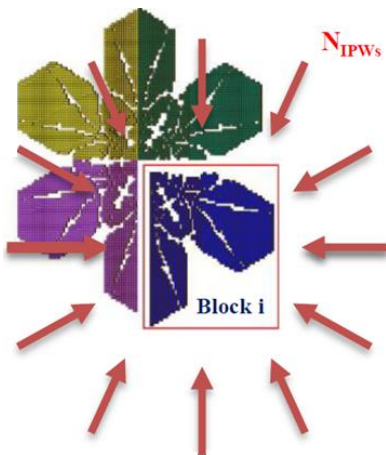


The main steps of the CBFM procedure presented in a distributed memory parallel configuration with a number of jobs equal to the number of blocks.

NESCoP



Non-uniform mesh depending on the size, shape and dielectric properties of the particles



$$Z^{ii} E_{MBFs}^{ii} = E_{IPWS}^{ii}$$

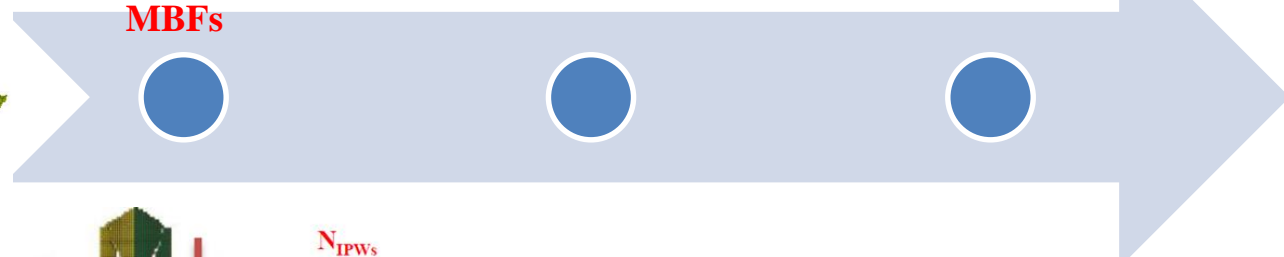
Diagonal/Sparse representation of the MBFs

Computing the CBFs for each block

$$Z^c = \begin{pmatrix} C^{(1)t} Z_{11} C^{(1)} & \dots & C^{(1)t} Z_{15} C^{(5)} \\ C^{(2)t} Z_{21} C^{(1)} & \dots & C^{(2)t} Z_{25} C^{(5)} \\ C^{(3)t} Z_{31} C^{(1)} & \dots & C^{(3)t} Z_{35} C^{(5)} \\ \vdots & \ddots & \vdots \\ C^{(5)t} Z_{51} C^{(1)} & \dots & C^{(5)t} Z_{55} C^{(5)} \end{pmatrix}$$

$K = S_1 + S_2 + S_3 + S_4 + S_5 \ll 3*N$

Solving the final reduced system of linear equation



Generation of the reduced matrix Z

Hybridization with the Adaptive Cross Approximation algorithm (ACA)

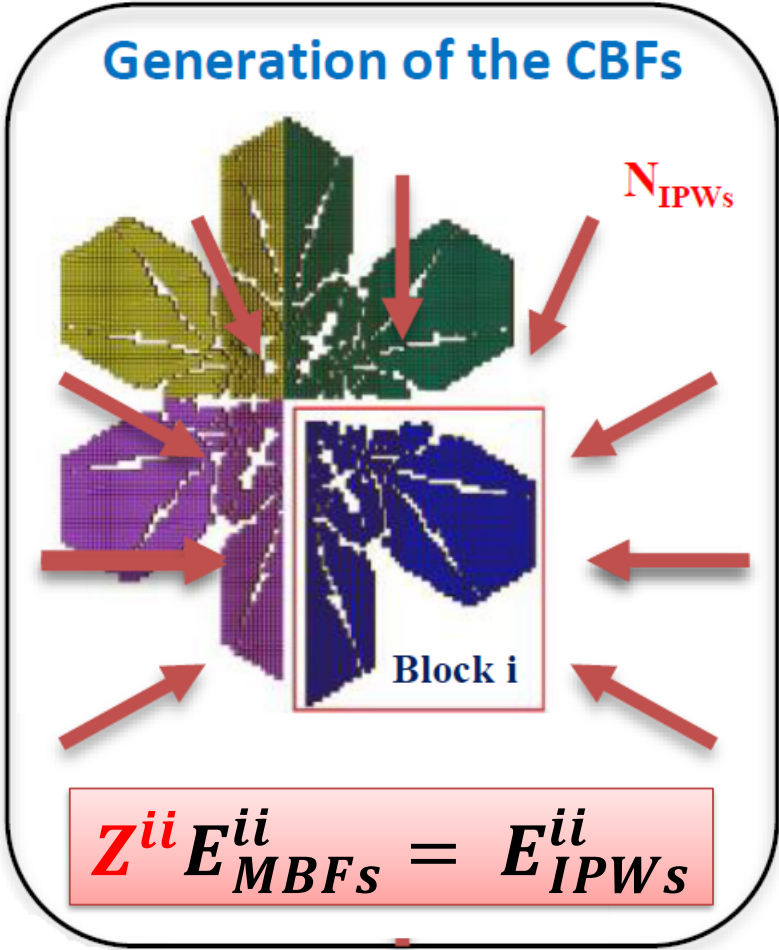
$$Z^c \alpha = V^c$$

by using a direct solver

Multi-Level CBFM-E
+
MPI parallelization of the CBFM code

Enhancement Techniques : Sparse Representation of the MBFs

After dividing the 3D complex geometry of the particle of N cells into M blocks



$$\tilde{Z}^{ii} E_{MBFs}^{ii} = E_{IPWs}^{ii}$$

$$\tilde{Z}_{l,c}^{ii} = 0$$

$$\text{if } |Z_{l,c}^{ii}| \leq |Z_{1,1}^{ii}| / f_{SR}$$

$$l, c = 1, \dots, 3Nb_c$$

f_{SR} is a threshold factor used to down-select the elements of Z^{ii} whose magnitudes are significant compared to $|Z_{1,1}^{ii}|$.

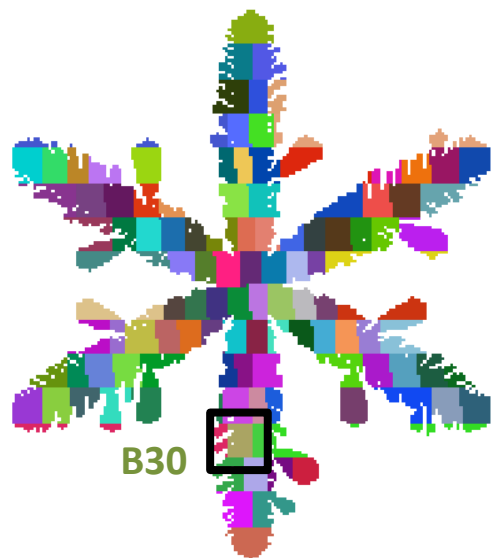
+

Sparse Direct Solver

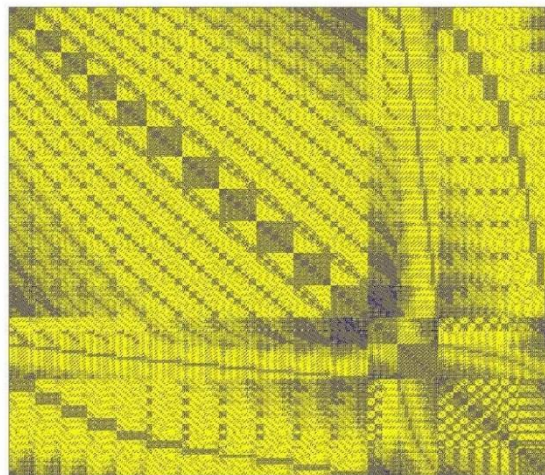


Make possible the use of larger blocks so a **higher CR**

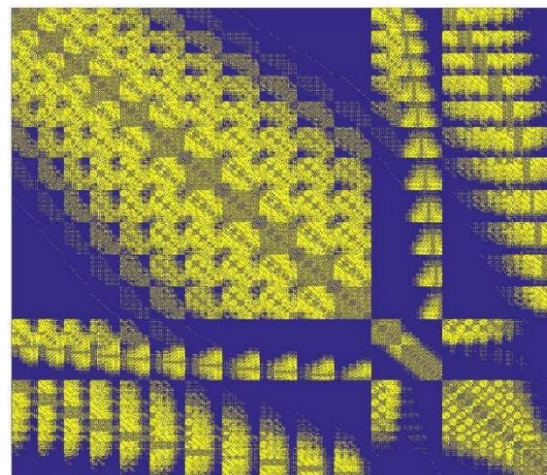
Enhancement Techniques : Sparse Representation of the MBFs



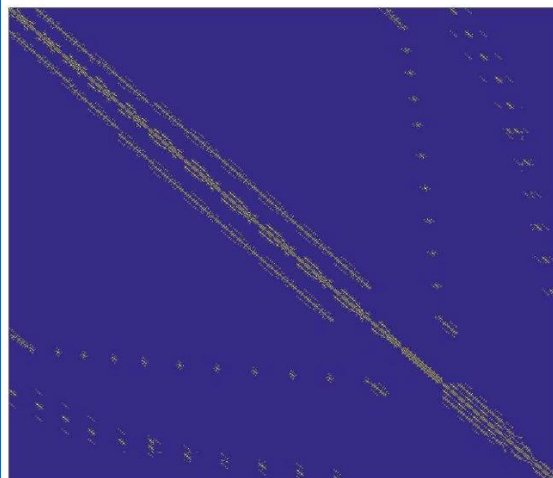
B30



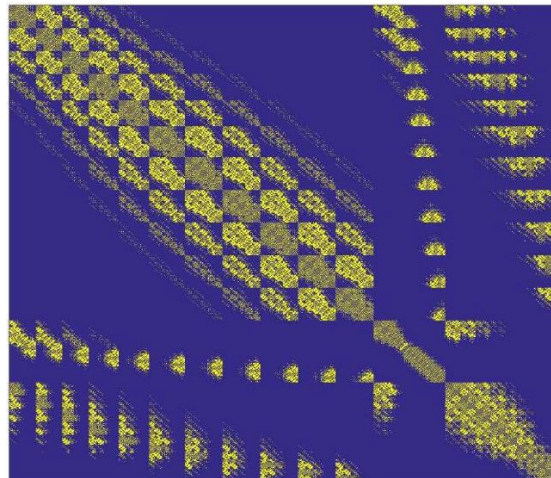
(a) $|Z^{ii}| \geq 10^{-4}$



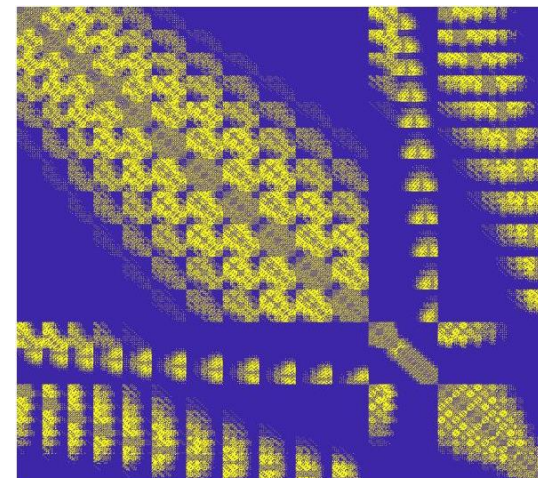
(b) $|Z^{ii}| \geq 10^{-3}$



(c) $|\tilde{Z}^{ii}|$ with $f_{SR} = 20$



(d) $|\tilde{Z}^{ii}|$ with $f_{SR} = 4 \times 10^2$



(e) $|\tilde{Z}^{ii}|$ with $f_{SR} = 10^3$

Numerical Analysis : NESCoP vs DDScat

Orientational averaging

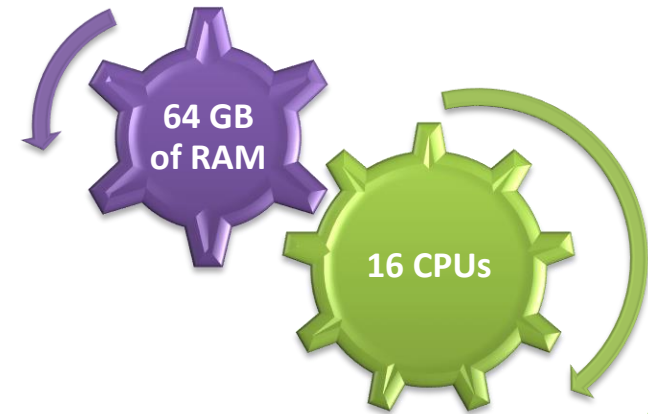
N $\langle Q \rangle = \frac{1}{4\pi} \int_0^{2\pi} d\phi_i \int_0^\pi \sin \theta_i d\theta_i Q(\phi_i, \theta_i)$

→ Incident directions (**id**)

D $\langle Q \rangle = \frac{1}{8\pi^2} \int_0^{2\pi} d\beta \int_{-1}^1 d \cos \theta \int_0^{2\pi} d\phi Q(\beta, \theta, \phi)$

→ Target orientations (**to**)

Shared Memory workstation

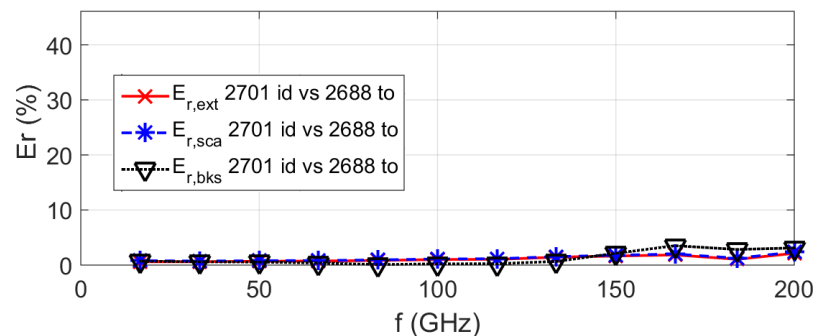
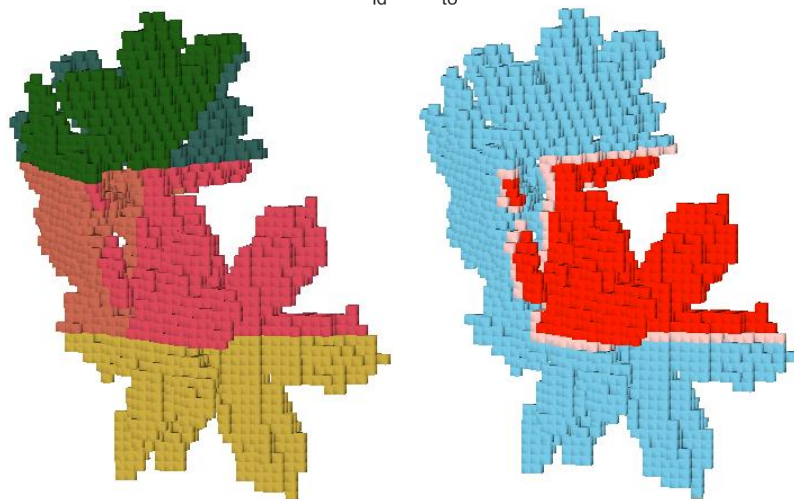
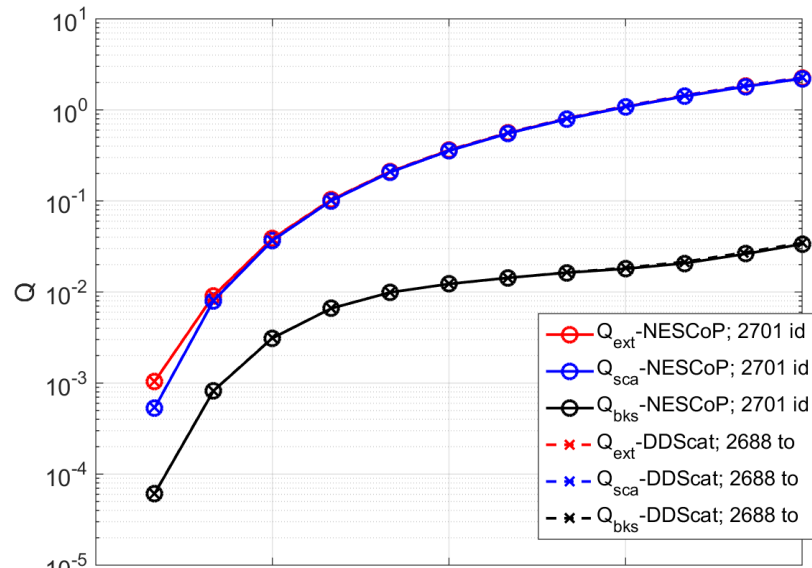
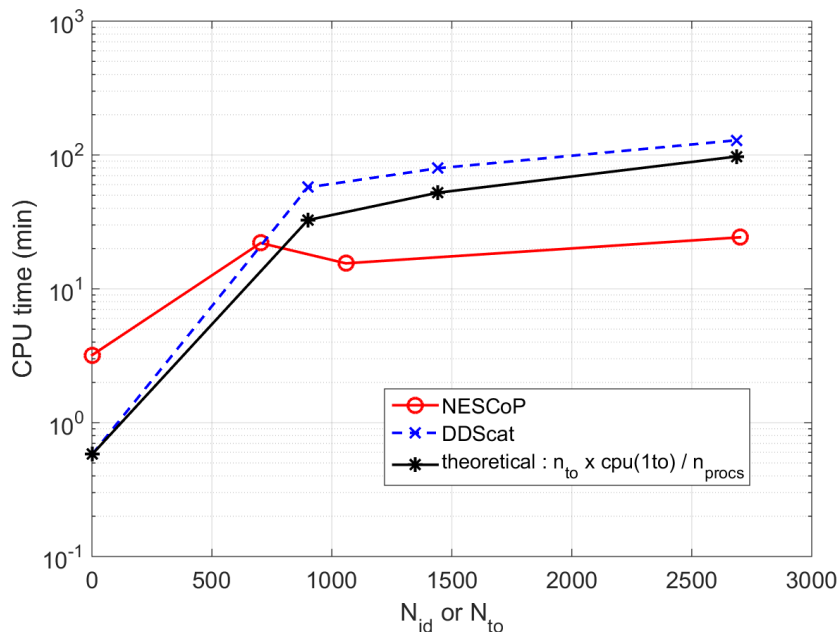


Relative 'difference' (per frequency)

$$E_{r,t}(\%) = 100 \times \frac{|Q_{t,NESCoP} - Q_{t,DDScat}|}{|Q_{t,DDScat}|}$$

Numerical Analysis : NESCoP vs DDScat

a0072



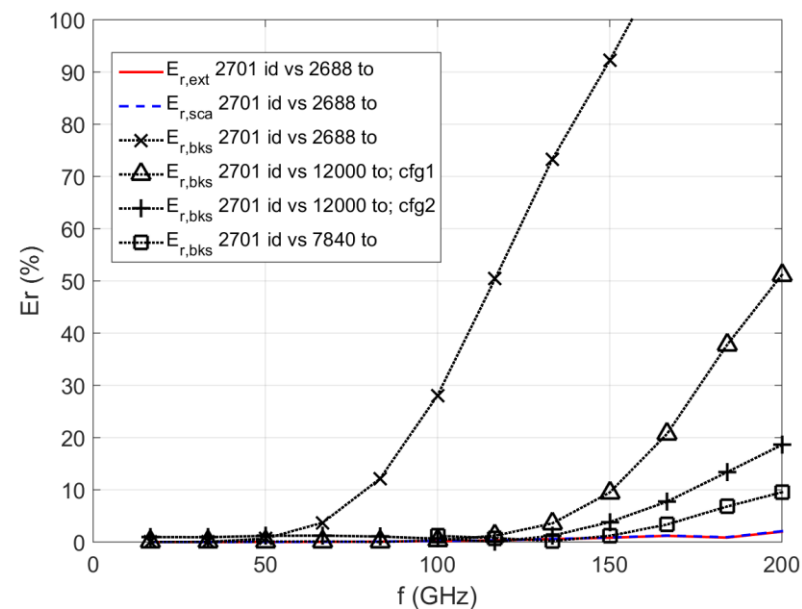
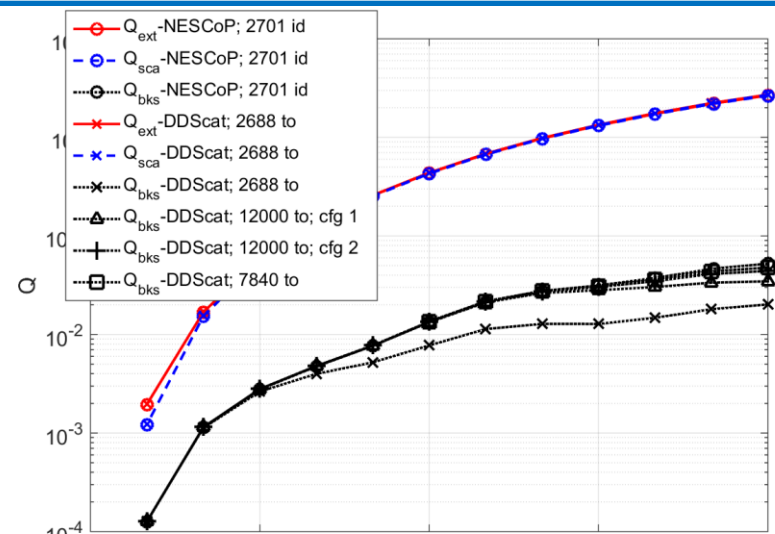
$a_p = 0.5 \text{ mm}; d_m = 2.55 \text{ mm}; 16 \leq f \leq 200 \text{ GHz} \rightarrow 0.17 \leq x_p \leq 2.09$
and $|m|kd \leq 0.37; N_b_c = 4159$

N_{to}	$N_{\beta}, N_{\theta}, N_{\Phi}$	$E_{r,ext/scat}$	$E_{r,bks}$	time
2688	16, 12, 14	2.05	159.2	65.37
14520	22, 30, 22	2.32	127.9	274.9
14616	58, 36, 7	2.34	107.9	562.17
10000	10, 50, 20	2.37	63.19	199.78
12000	8, 60, 25	2.36	51.15	213.5
12000	30, 80, 5	2.39	18.6	607.32
5700	60, 95, 1	2.4	13.04	1182
7840	80, 98, 1	2.39	9.52	1974.6

Time (min) and maximum relative difference (%) obtained with DDScat for the ice pristine p08 in comparison to NESCoP with 2701 id, depending on the number of target orientations N_{to} and on their distribution.



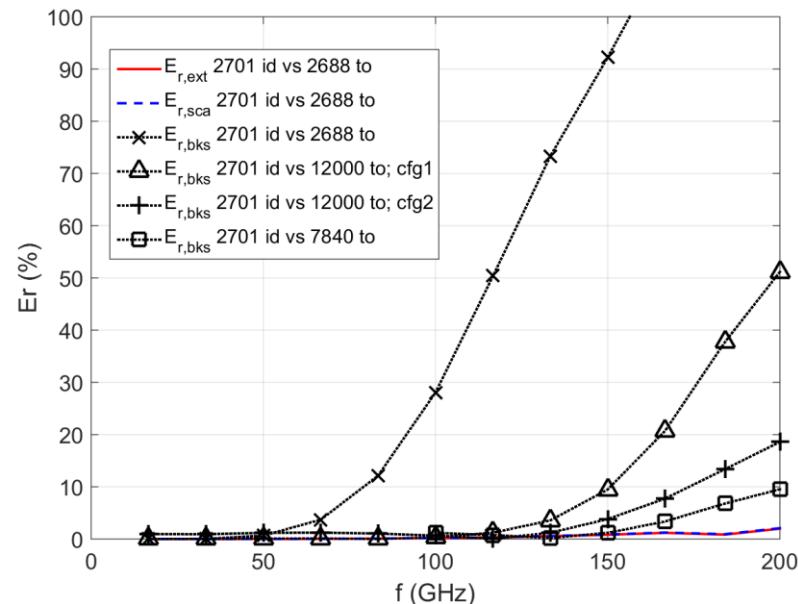
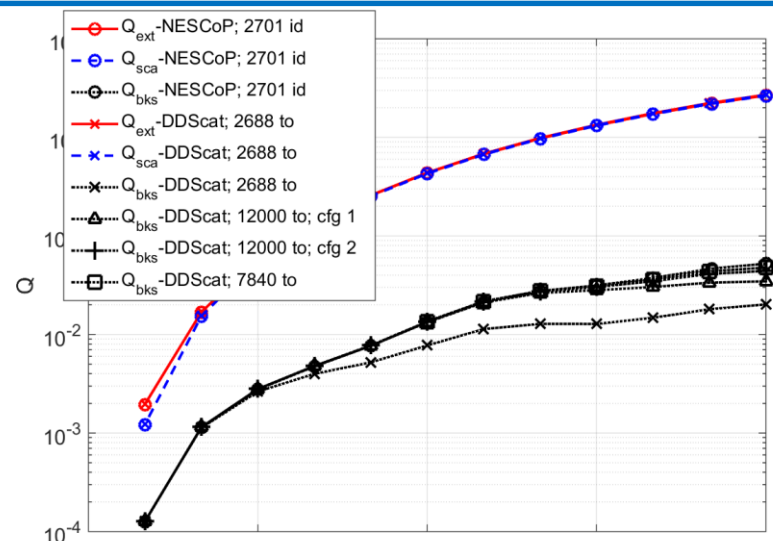
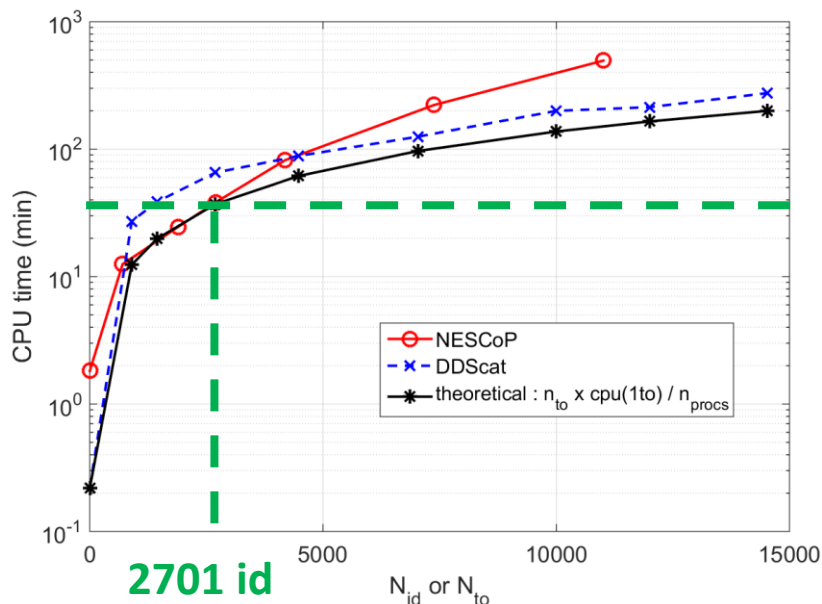
$a_p = 0.58 \text{ mm};$
 $d_m = 4.30 \text{ mm};$
 $0.2 \leq x_p \leq 2.49$ and
 $|m|kd \leq 0.37 ;$
 $Nb_c = 6738$

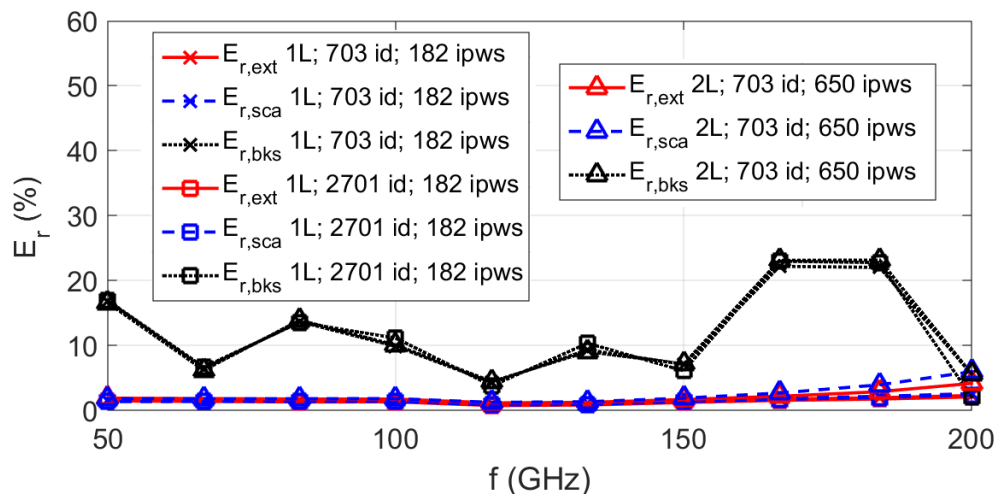
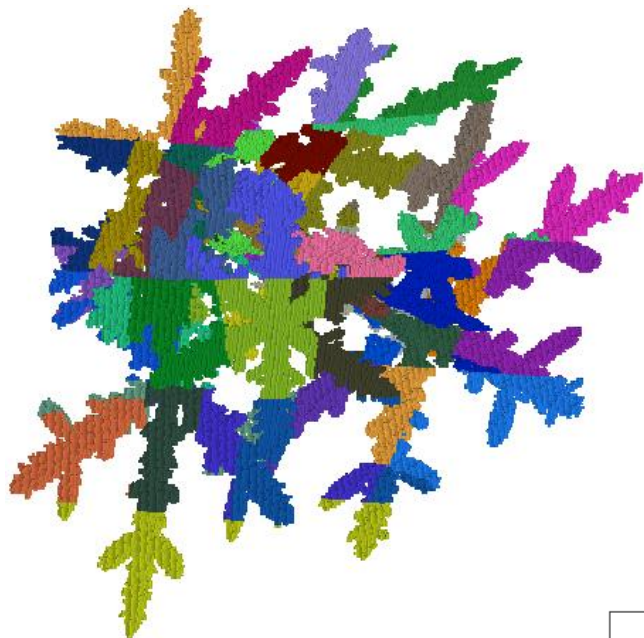




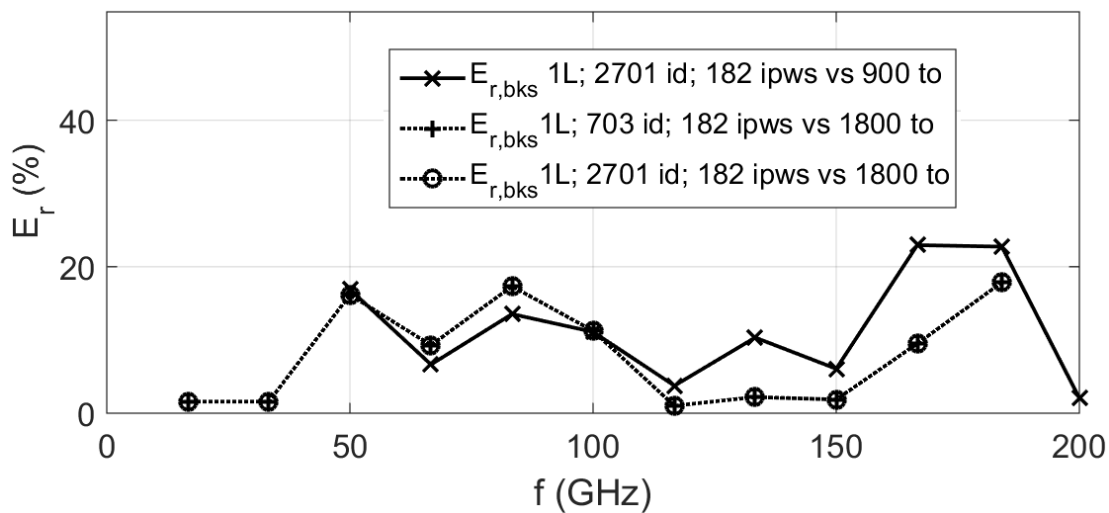
N_{to}	$N_{\beta}, N_{\theta}, N_{\phi}$	$E_{r,ext/scat}$	$E_{r,bks}$	time
2688	16, 12, 14	2.05	159.2	65.37
14520	22, 30, 22	2.32	127.9	274.9
14616	58, 36, 7	2.34	107.9	562.17
10000	10, 50, 20	2.37	63.19	199.78
12000	8, 60, 25	2.36	51.15	213.5
12000	30, 80, 5	2.39	18.6	607.32
5700	60, 95, 1	2.4	13.04	1182
7840	80, 98, 1	2.39	9.52	1974.6

Time (min) and maximum relative difference (%) obtained with DDScat for the ice pristine p08 in comparison to NESCoP with 2701 id.





$a_p = 1.61 \text{ mm};$
 $d_m = 11.45 \text{ mm};$
 $0.56 \leq x_p \leq 6.74$
 $|m|kd \leq 0.37$
 $Nb_c = 140896 \text{ cells}$



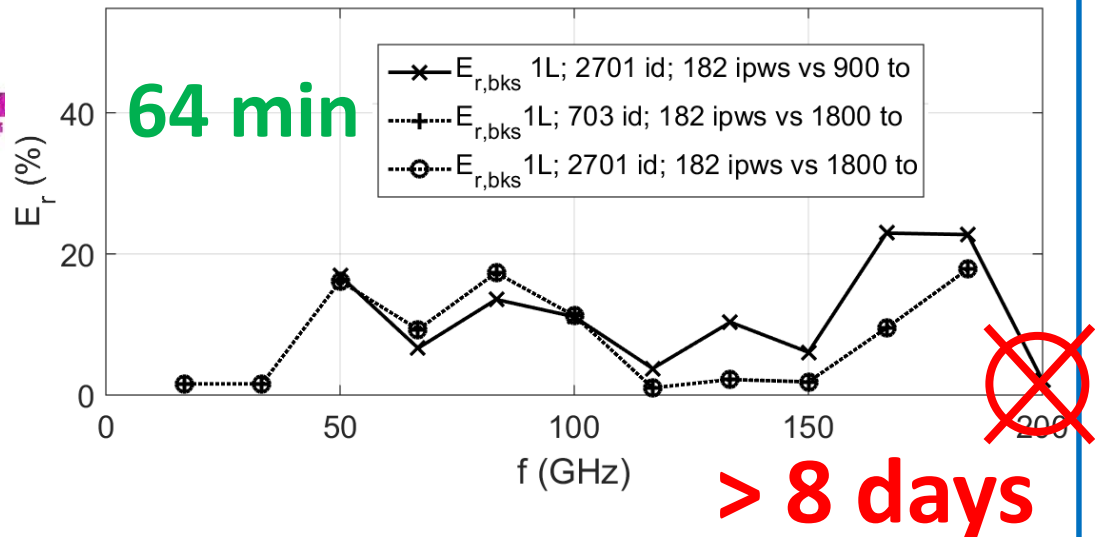
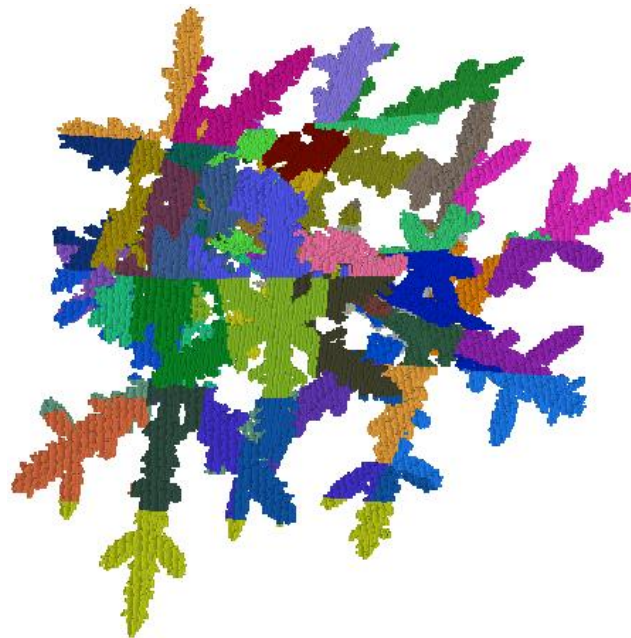


TABLE : CPU time (min) needed by NESCoP, with 1L and 2L CBFM-E, and DDScat to calculate averaged scattering by a0006 with 703 and 2701 **id** and 900 and 1800 **to** for $16.67 \text{ GHz} \leq f \leq 200 \text{ GHz}$.

165

	1 id/to	703 id	900 to	1800 to	2701 id
1L CBFM-E	126.72	527.67	–	–	1706
2L CBFM-E	329.47	532.15	–	–	1034.87
DDScat	266	–	39207	≥ 85860	–

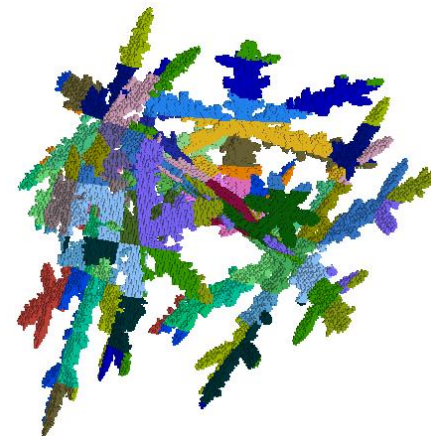
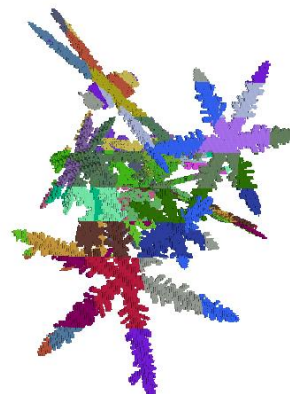
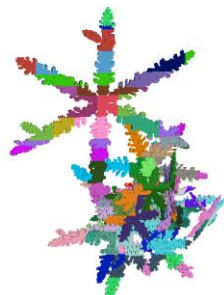


NESCoP



3D full wave model comparable to the DDA in terms of accuracy when providing **higher computational performance** particularly with orientational averaging of the EM scattering.

- ❖ MPI parallelization of the codes
- ❖ Exploring other techniques for efficient calculation of the CBFs
- ❖ Implementation of the wideband code for the CBFM





Thanks for your attention



ScaLAPACK - Scalable Linear Algebra PACKage

is a library of high-performance linear algebra routines for **parallel distributed memory machines**. It solves **dense and banded linear systems**, least squares problems, eigenvalue problems, and singular value problems

1	2	5	6	9					
10	11	14	15	18					
37	38	41	42	45					
46	47	50	51	54					
73	74	77	78	81					

Process 0 : (0,0)

3	4	7	8						
12	13	16	17						
39	40	43	44						
48	49	52	53						
75	76	79	80						

Process 1 : (0,1)

19	20	23	24	27					
28	29	32	33	36					
55	56	59	60	63					
64	65	68	69	72					

Process 2 : (1,0)

21	22	25	26						
30	31	34	35						
57	58	61	62						
66	67	70	71						

Process 3 : (1,1)

$$Z^c = \begin{pmatrix} C^{(1)t} Z_{11} C^{(1)} & \dots & C^{(1)t} Z_{15} C^{(5)} \\ C^{(2)t} Z_{21} C^{(1)} & \dots & C^{(2)t} Z_{25} C^{(5)} \\ C^{(3)t} Z_{31} C^{(1)} & \dots & C^{(3)t} Z_{35} C^{(5)} \\ \vdots & \ddots & \vdots \\ C^{(5)t} Z_{51} C^{(1)} & \dots & C^{(5)t} Z_{55} C^{(5)} \end{pmatrix}$$

2-D partitioning



Solving the reduced matrix equation



Enhancement Techniques : MPI parallelization

JPL

JPL IT | The Lab's Information Technology Resource and Service Gateway

HIGH PERFORMANCE COMPUTING

- Home
- Team

RESOURCES

- JPL Operated Resources
- - **Zodiac**
- - Aurora and Halo
- NASA Advanced Supercomputing
- San Diego Supercomputer Center
- Amazon Cloud

Zodiac

The Zodiac supercomputer is an SGI Altix ICE 8400LX cluster, with a scalable distributed-memory multiprocessor system that is tuned for Message Passing applications. Zodiac supports parallel programming with the message-passing interface (MPI).

Software Tools >>

Hardware Specifications <<

Compute Node Specifications:

- 1 login node
- 160 Compute nodes
 - 1920 Total Cores
 - Dual-socket, 6-core, 2.66 GHz Intel Xeon X5650 (Westmere) CPUs
 - 12 cores per node
 - 12MB L3 cache memory per core
 - 24GB (2GB/core) DDR3 memory per node

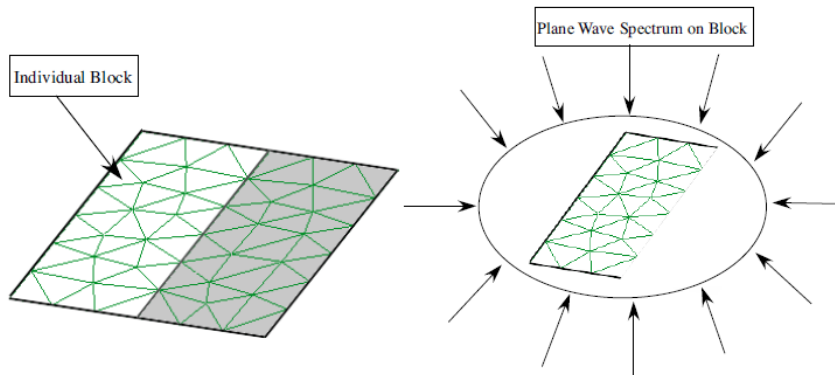
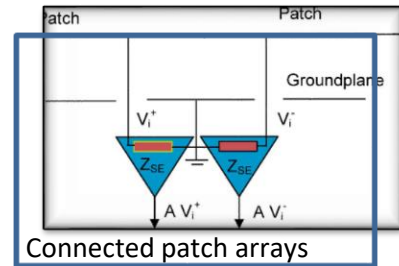
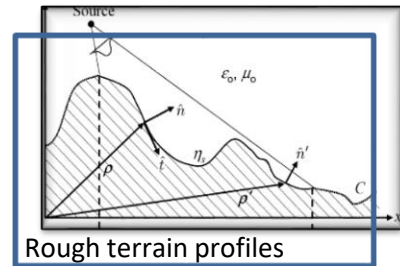
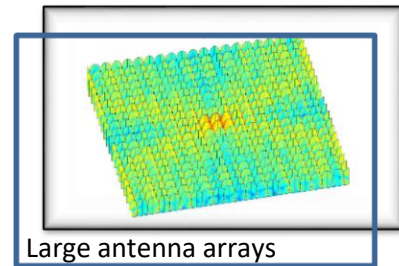
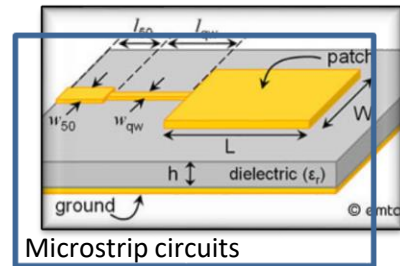
The Characteristic Basis Function Method (CBFM)

Direct solver-based

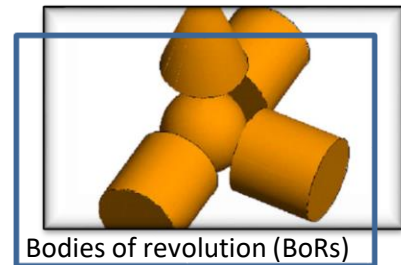
To overcome the limitation caused by the use of a MoM, we employ the **CBFM** which has been proven to be accurate and efficient when applied to large-scale EM problems, even when the computational resources are limited

CBFM

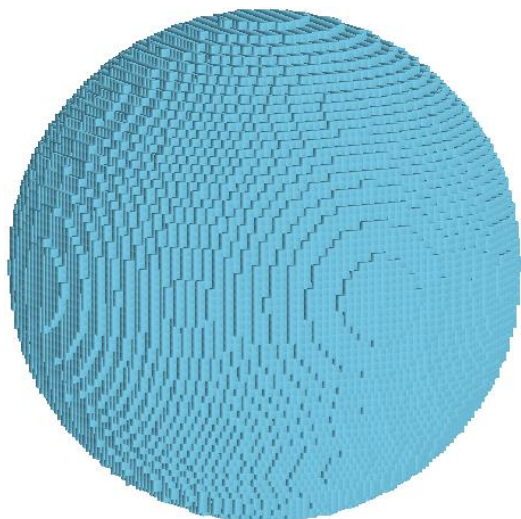
- ❖ Better adapted to **multiple right-hand** side problem
- ❖ Subject to a wide variety of enhancement techniques
- ❖ Tunable depending on to the needs (memory or CPU) through the size of the blocks (h_B or $N_{b,max}$).
- ❖ Highly amenable to **MPI** parallelization



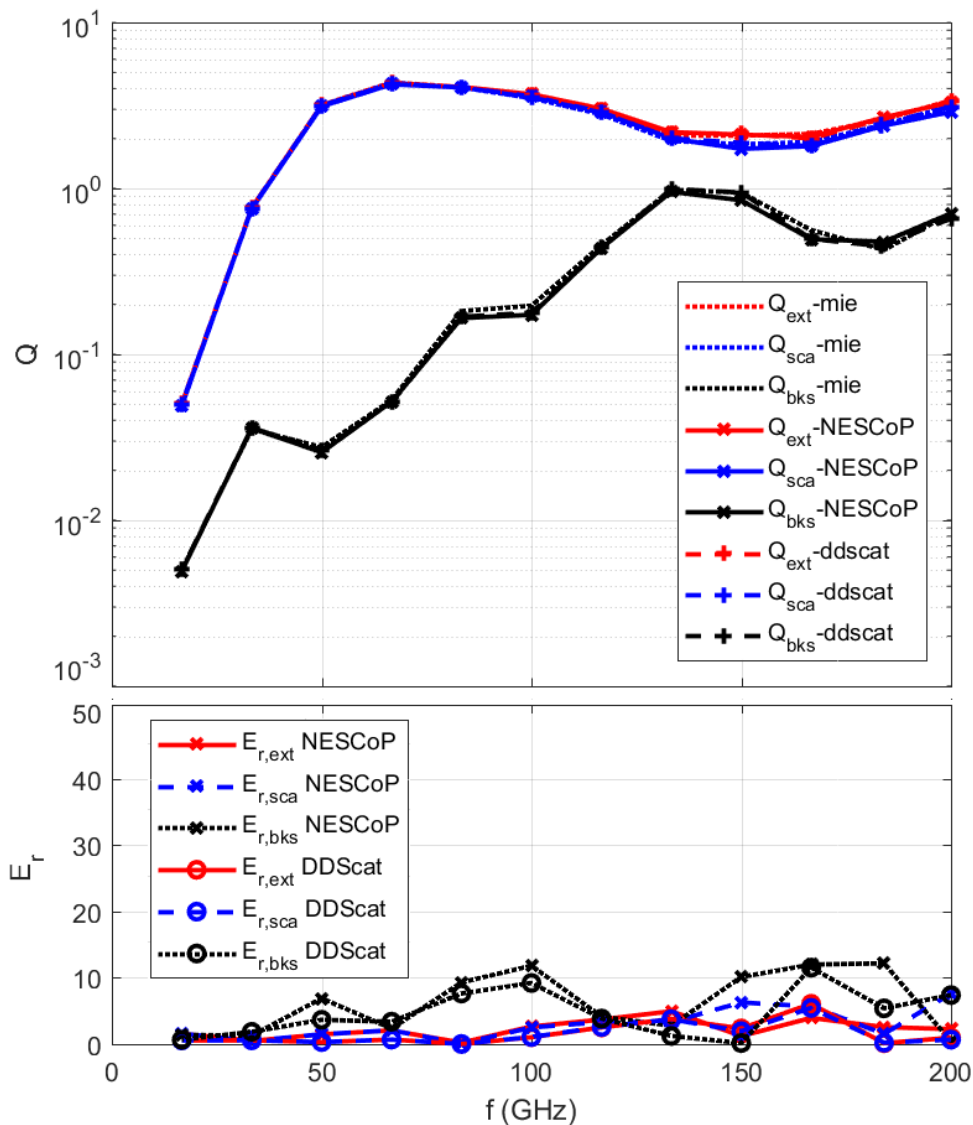
Spectrum of plane waves incident on a single block

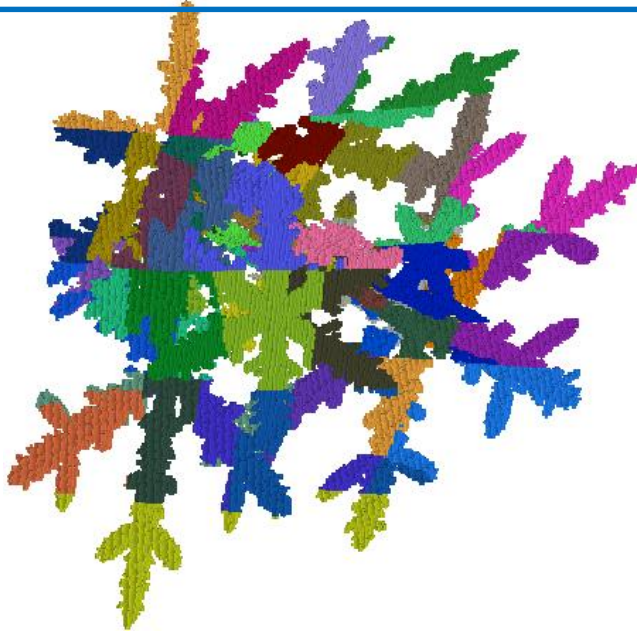


Sphere : NESCoP vs DDScat vs Mie theory



$a_p = 1.6 \text{ mm};$
 $0.55 \leq x_p \leq 6.7$
 $|m|kd \leq 0.37$
 $Nb_c = 137376 \text{ cells}$





$a_p = 1.61 \text{ mm};$
 $d_m = 11.45 \text{ mm};$
 $0.17 \leq x_p \leq 6.74$
 $|m|kd \leq 0.37$
 $Nb_c = 140896 \text{ cells}$

TABLE III: Relative difference $E_{r,t}(\%)$ and computational performance (CPU time in minutes, size of Z^c and compression rate) when calculating averaged scattering by a0006 with 2701 **id** at $f = 150 \text{ GHz}$, depending on the use or not of the DR and SR techniques, on h_B and f_{SR} . $\langle Nb_e \rangle$ refers to the average extended block size and $p_{i,sr} (\%)$ is the stored proportion (in percentage) of the sparse self-coupling MoM sub-matrix Z^{ii}

$h_B \rightarrow \langle Nb_e \rangle$	DR/SR; f_{SR}	$\max(p_{i,sr})$	size of Z^c	CR	CBFs (min)	$(Z^c)^{-1}$ (min)	$E_{r,ext}$	$E_{r,scat}$	$E_{r,bks}$
1.0 mm \rightarrow 594	DR/SR=0	–	17795	23.7	32	444.3	0.99	0.6	0.53
2.4 mm \rightarrow 3509	DR/SR=0	–	5311	79.6	341.8	161	1.13	0.37	1.03
	DR=1	–	5614	75.3	4.18	165	7.79	6.99	8.36
	SR=1; 10^2	0.31	5582	75.7	5.3	162.7	3.4	2.66	3.82
	SR=1; $2 \cdot 10^2$	0.59	5547	76.2	6.08	160	2.58	1.86	2.89
	SR=1; 10^3	2.21	5465	77.3	13.6	84.5	1.67	0.98	1.88
	SR=1; 10^4	22.68	5319	79.5	68	151	1.14	0.36	1.02

